Electron-impact excitation of the doubly excited states of helium below the $N=3$ He^+ threshold

S. J. Brotton, S. Cvejanovic,* F. J. Currell,† N. J. Bowring, and F. H. Read
Department of Physics and Astronomy, Schuster Laboratory, Manchester University, Manchester M13 9PL, United Kingdom
(Received 5 April 1996)

Measurements of the doubly excited states of helium below the $He^+(N=3)$ threshold populated by electron impact are presented for a range of scattering angles and residual energies. The deduced values of the energies and widths for 11 of the optically forbidden states are compared with theoretical values, which shows the agreement to be good for the energies but poorer for the widths. The data verify propensity rules in Lin's [Adv. At. Mol. Phys. **22**, 77 (1986)] *K*, *T*, *A* classification scheme for the cross sections. By comparing the $2s^2\ ^1S^e$ and $3s^2\ ^1S^e$ states at the scattering angle of 20° and the residual energy of 40 eV, we obtain a dependence of $n^{-10.1\pm0.8}$ for the cross section at these conditions. [S1050-2947(96)09112-3]

PACS number(s): 34.80.Dp, 32.80.Dz, 31.50.+w, 31.25.Jf

I. INTRODUCTION

The doubly excited states of helium are fundamental systems for the investigation of electron-electron correlations [1]. The two electrons in these states are highly correlated, since the strength of the electron-electron interaction is comparable to the electron-nucleus interaction. Due to the increasing release from the effects of the nucleus, the importance of electron-electron correlations rises for higher values of the principle quantum number n of the two excited electrons. Therefore, the doubly excited states cannot be classified by the independent-particle model, and interpretation requires the use of the quantum numbers of the pair of electrons (see Sec. III A). The doubly excited states lie above the single-ionization threshold and so decay by autoionization [2].

The first evidence for these correlation effects was provided by Madden and Codling [3] who used synchrotron radiation to observe a full series of doubly excited $^1P^o$ levels converging to the $He^+(N=2)$ limit. Later observations using the same technique include those of Woodruff and Samson [4] who observed the states converging to the $N=3$, 4, and 5 limits, and the measurements of Domke *et al.* [5] below the $N=2$–8 thresholds. By contrast to the rapid progress of the photoelectron experiments to higher energies, the doubly excited states had only been measured by electron-impact excitation below the $N=2$ ionization limit [6] before the present work. The great advantage of electron-impact spectroscopy is that, unlike the photon experiments, it is possible to observe both the optically allowed and forbidden transitions and so to reveal the full richness of the spectrum. The $N=3$ states had not been observed in electron-impact experiments for two main reasons. First, as will be shown, the cross sections of doubly excited states decrease rapidly with increasing N. Second, the amplitudes of the resonance structures are less than 5% of the cross section of the direct-ionization process, and so it is necessary to see the states above the relatively large random fluctuations of the continuum. As a result, very long collection times are required to obtain adequate statistics.

There are three main aims of the experiment. First, to provide the initial measurements of the energies and widths of states with a wide range of quantum numbers for comparison with theoretical values. Second, to investigate how the relative cross sections of the doubly excited states depend upon their pair quantum numbers. Third, to determine how the cross sections of the "ns^2" $^1S^e$ states vary with n, since this provides information about how the two electrons are correlated.

II. EXPERIMENTAL DETAILS

A. The spectrometer

The electron spectrometer has been described in detail elsewhere [7], and so only a brief discussion is given here. The electrons are produced by a heated tungsten filament and are transported through the system using stacks of triple aperture electrostatic lenses [8]. A hemispherical deflection monochromator produces an electron beam with a narrow energy spread, which is focused onto a gas beam effusing from a hypodermic needle. The energies of the electrons scattered from the interaction region are measured by a hemispherical deflection analyzer. In order to observe at different scattering angles, the analyzer can be rotated between $-10°$ and 100° with respect to the direction of the incident electron beam. The energy analyzed image at the exit plane of the analyzer is recorded by a multidetector [9]. The multidetector gives a great increase in the data collection efficiency, which is necessary since the $N=3$ states have very small cross sections. The spectra are typically collected over a period of a week, and several such spectra are then added together to give those presented below.

The spectra are collected in the constant residual energy mode, in which the impact energy is ramped by a sawtooth voltage while the voltage of the residual energy power supply is fixed. The energy scale is unaffected by field penetration into the interaction region, and so the measured energies are more accurate than in ejected electron spectroscopy. The drifts in the energy-loss scale were random with a root-mean-square deviation of 4.5 meV. The energy-loss scale

*Present address: Department of Physics, University of Newcastle, Newcastle-Upon Tyne NE1 7RU, UK.
†Present address: Institute for Laser Science, University of Electro-Communications, Tokyo, Japan.

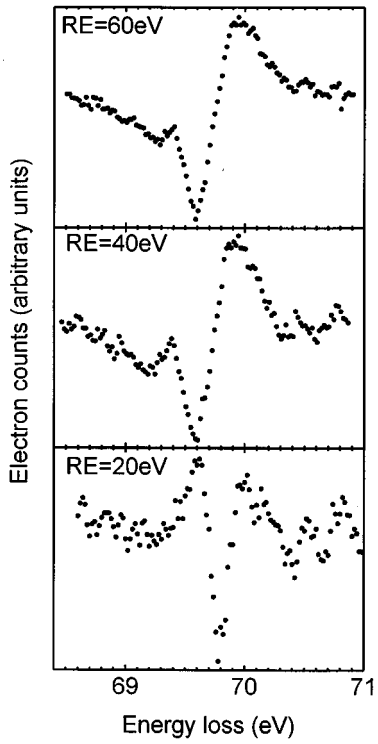

FIG. 1. The variation of the low resolution $N=3$ spectra with residual energy RE when the scattering angle is 20°.

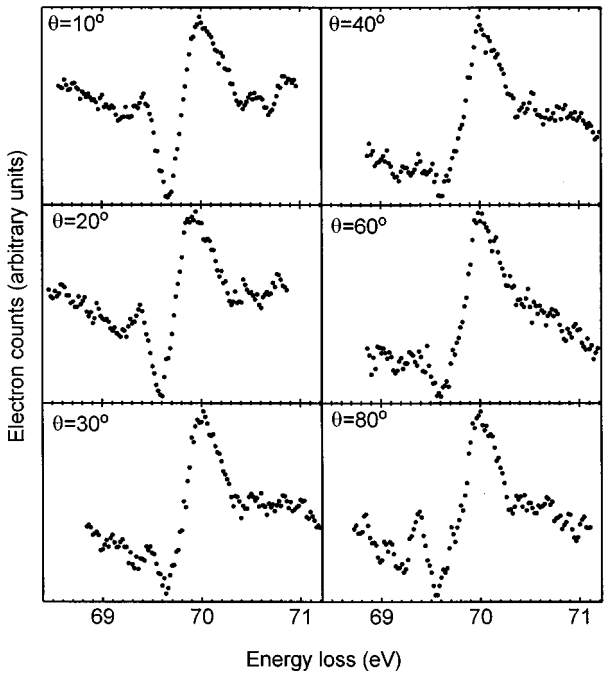

FIG. 2. The variation of the low resolution $N=3$ spectra with the scattering angle θ when the residual energy is 40 eV.

was calibrated using the $2\,^1S$ state of helium.

A small fraction of the electrons in the incident beam scatter inelastically from structural parts of the target region, and also some electrons escape from the sides of the electron optical systems. Consequently, some of the counts in the energy-loss spectra originate from sources other than the gas beam, and this yield will be referred to as the background (not to be confused with the direct-ionization continuum). Therefore, to measure the cross section it is essential to know the fraction of the total count rate due to the background (see Sec. VI), which is achieved by introducing the gas into the chamber via an alternate route and then remeasuring the count rate. The background is found to be negligible for all the spectra to be discussed.

B. Choice of incident energies and scattering angles

In the first stage of the experiment, the $N=3$ spectra are collected at different scattering angles and residual energies to find the experimental conditions that allow the data to be most easily interpreted. To complete this first stage within a reasonable time, the pass energies of both the monochromator and analyzer were raised to the high value of 11 eV, which leads to the low-energy resolution of approximately 110 meV. In the second stage of the experiment, the optimum conditions are repeated at the improved energy resolution of 60 meV, as discussed in Sec. IV.

We start by examining the variation of the spectra with residual energy for a fixed scattering angle, which was chosen as 20° because this was found to be the most suitable condition for the $N=2$ data [10]. In Fig. 1 the spectra are shown at the residual energies of 20 eV, 40 eV, and 60 eV. When the residual energy is increased from 40 eV to 60 eV there is little change in the spectrum, although the relative cross section of the peak at about 69.4 eV reduces slightly. It will be shown in Sec. IV that this peak is due to the $_3(2,0)_3^+\,^1S^e$ and $_3(2,0)_3^+\,^3P^o$ states (using Lin's classification scheme, see Sec. III A), which appear merged in Fig. 1 because of the low resolution. The energy, width, and cross section of the $_3(2,0)_3^+\,^1S^e$ state are of particular interest (see Sec. VI), and so the collection energy of 40 eV should be chosen in preference to 60 eV. Residual energies higher than 60 eV are likely to be less interesting, since as the impact energy is raised the optically forbidden cross sections decrease. The change in the spectrum when the residual energy is reduced from 40 eV to 20 eV is much more dramatic, because a large resonance profile becomes prominent at about 69.7 eV, which is interpreted in Sec. IV as a sudden increase in the relative cross section of the $_3(2,0)_3^+\,^1D^e$ state. In general, much more structure is visible at 20 eV than 40 eV. The time required to obtain adequate statistics is significantly longer at 20 eV than 40 eV, and so spectra with residual energies lower than 20 eV were not collected.

Next we consider the variation of the spectra with angle. The $_3(2,0)_3^+\,^1S^e$ state is of special interest, and also it is desirable to minimize the collection time, and so a suitable fixed residual energy is 40 eV. Figure 2 shows the spectra at 10°, 20°, 30°, 40°, 60°, and 80°, and reveals that the structure varies little with the angle. The most noticeable change is in the peak at about 69.4 eV due to the merged $_3(2,0)_3^+\,^1S^e$ and $_3(2,0)_3^+\,^3P^o$ states, which is prominent at 20° and 80° but is barely visible at 30°, 40°, and 60°. Thus, the figures show that the angles most likely to give the energies and widths of the $_3(2,0)_3^+\,^1S^e$ and $_3(2,0)_3^+\,^3P^o$ states are 10°, 20°, and 80°. Considering the signal and back-

ground count rates, the most suitable scattering angle is 20°.

In summary, if the aim is to determine the energies and widths of the ${}_3(2,0)_3^+\ {}^1S^e$ and ${}_3(2,0)_3^+\ {}^3P^o$ states, then the residual energy should be 40 eV and the scattering angle 20°, whereas if the ${}^1D^e$ states, and possibly other optically forbidden states, are of interest then a residual energy of 20 eV and a scattering angle of 20° are suitable.

C. Fitting the data

To fit to the experimental data, it is necessary to convolve the theoretical line shapes with the apparatus function G in order to represent the imperfect energy resolution of the spectrometer. Using the singly and $N=2$ doubly excited states, we carefully investigated the shape of G and found it to be accurately approximated by a single Gaussian. Therefore, to obtain the energies E_{mk}, widths Γ_{mk}, and the shapes and amplitudes of the noninterfering resonance profiles (see Sec. III B), the experimental data are fitted to the formula

$$I(E_0)=\int_{-\infty}^{\infty}\frac{d\sigma}{d\Omega}G(W,E-E_0)dE, \tag{1}$$

where [11]

$$\frac{d\sigma}{d\Omega}=C(E)+\sum_k\frac{A_{mk}(E-E_{mk})+B_{mk}(\Gamma_{mk}/2)}{(E-E_{mk})^2+(\Gamma_{mk}/2)^2}. \tag{2}$$

Here the subscript m signifies a measured value, W is the full width at half maximum of the Gaussian apparatus function, $C(E)$ is a quadratic function of the energy loss and accounts for both the variations in the cross section of the direct-ionization continuum and the detection efficiency of the spectrometer, and the A_{mk} and B_{mk} are the Shore parameters. The E_{mk}, Γ_{mk}, A_{mk}, and B_{mk} are obtained using Marquardt's method [12].

For the nonlinear parameters E_{mk} and Γ_{mk}, the error ε_{mk} is defined by [13]

$$\chi^2(a_{mk}+\varepsilon_{mk})=\chi^2(a_{mk})+1, \tag{3}$$

where a_{mk} is the value of E_{mk} or Γ_{mk} that gives the minimum χ^2. The ε_{mk} are obtained by the Marquardt method. The errors to be quoted in Table I also include the inaccuracy due to random drifts in the energy loss scale and the uncertainty in the apparatus function W.

III. THEORY

A. Propensity rules

In order to interpret the spectra, it is necessary to know the theoretical energies E_t and widths Γ_t of the $N=3$ states. Over the past few decades, there have been many calculations of E_t and Γ_t, some of the most accurate and extensive of which are those by Ho and co-workers [14]. The calculations of [14] show that there are many broad and closely spaced states in the present energy range. Consequently, there is a large overlap between the states, which makes the interpretation of the spectra difficult. We therefore discuss propensity rules that allow the number of states included in the data analysis to be greatly reduced.

By considering the correlation between the two electrons in the doubly excited states, propensity rules for autoionization and radiative excitation and decay have been derived using the molecular-orbital model [15,16] and the hyperspherical coordinate method [17,18]. We use the hyperspherical classification scheme of Lin in which the correlated wave function is represented by the notation ${}_n(K,T)_N^{A\ 2S+1}L^{\Pi}$; where L, S, and Π are the usual quantum numbers; n is the principle quantum number of the outer electron; and K,T,A are the correlation quantum numbers [19]. In Lin's classification scheme, in order to represent the correlated motion of the two excited electrons the coordinates are chosen as the distances r_1 and r_2 of the electrons from the nucleus and the interelectronic angle $\theta_{12}=\hat{r}_1\cdot\hat{r}_2$. The quantum number K describes the angular correlation of the two electrons or the dependence of the wave function on θ_{12}, and is given by

$$K\approx\langle r_<\cos\theta_{12}\rangle, \tag{4}$$

where $r_<$ is the radius of the inner electron. If K has its maximum possible value, then the two electrons are localized on opposite sides of the nucleus. T is equal to the projection of the total angular momentum onto the interelectronic axis. When $T=0$ the two electrons move in the same plane and as T increases the angle between the orbital planes rises. Herrick and Sinanoglu showed that the possible values of K and T for a given N, L, and Π are restricted by [20]

$$T=0,1,2,\ldots,\min(L,N-1),\quad \text{if } \Pi=(-1)^L$$

$$K=N-1-T,\quad N-3-T,\ldots,-(N-1-T). \tag{5}$$

The quantum number A was added to represent the radial correlations of the two electrons. When $A=+1$ the radial oscillations of the two electrons are in phase, whereas for $A=-1$ the electrons oscillate out of phase. If $A=0$ then there is little radial correlation and the states are similar to the singly excited configurations.

To apply the ideas of [17] for autoionization to the electron-impact excitation from the ground state, we use the approximation that the partial width for the decay to the $He^+(N=1)$ channel is proportional to the cross section for the inverse excitation process. Arguments essentially equivalent to those of [17] then yield the following propensity rules for K, T, and A:

(1) The states with $A=+1$ will have much the largest excitation probability, followed by, in order of decreasing cross section, those with $A=-1$ and $A=0$, respectively. Since $A=+1$ for the ground state, the propensity rule becomes $\Delta A=0$. It is also expected that the widths of the $A=-1$ configurations are very much smaller than those of the $A=+1$ states.

(2) For a given T, A, and ${}^{2S+1}L^{\Pi}$, as K becomes more positive, the excitation probability increases. Thus, for example, the ${}_3(2,0)_3^+\ {}^1D^e$ state will be easier to excite than the ${}_3(0,0)_3^+\ {}^1D^e$ state, and the ${}_3(0,0)_3^+\ {}^1D^e$ state will, in turn, have a larger cross section than the ${}_3(-2,0)_3^+\ {}^1D^e$ state. However, one possible exception to this trend is the ${}_3(2,0)_3^+\ {}^1S^e$ and ${}_3(0,0)_3^+\ {}^1S^e$ pair [17], since for the related case of the total widths the ratio of the theoretical values is

1:2.2 [14]. Therefore, rather than applying the K propensity rule to the possibly anomalous ${}_3(0,0)_3^+\ {}^1S^e$ state, the spectra are examined to search for its presence.

(3) For a given K, A, and ${}^{2S+1}L^{\Pi}$, the larger T the greater is the cross section.

(4) The effect of A on the cross section is stronger than that of K, and the effect of K is greater than that of T.

We provide some physical insight into propensity rules 1, 2, and 3. When $A=-1$ the electrons oscillate out of phase, so that if one electron is close to the nucleus the other is distant. By contrast, the two electrons are either simultaneously close to or far from the center of the atom for the in-phase oscillations of states with $A=+1$. Therefore, when $A=+1$ the probability of finding *both* electrons close to the nucleus is significantly higher than if $A=-1$, which leads to a greater overlap with the initial ground state $1s^2$ and hence to a larger cross section. We thus obtain propensity rule 1. As K becomes more negative, the electrons are on average separated by a smaller angle θ_{12}, which results in a larger electron-electron repulsion. There is also an increase in the electron-electron repulsion when T reduces, since the probability of close encounter between the two electrons is greater if the angle between the orbital planes is smaller. In both cases, the higher electron-electron repulsion causes the atomic size to increase, which leads to a reduction in the amplitude of the doubly excited state wave function in the center of the atom and so to a smaller cross section. Thus the larger K and T the greater is the cross section, which gives propensity rules 2 and 3.

As a guide to how the cross sections of the $N=3$ states vary with S, L, and Π, the experimental spectra for the doubly excited states of helium below the $N=2$ threshold can be used. These spectra, collected at the same scattering angles and residual energies as the data for $N=3$, show that the ${}^1D^e$ and ${}^1P^o$ states have the largest cross sections, followed by the ${}^1S^e$ and ${}^3P^o$ states. Thus, the $N=2$ spectra are dominated by the P and D states. A similar dependence on ${}^{2S+1}L^{\Pi}$ is expected for the $N=3$ states.

A transition for which

$$\Delta L+\Delta\Pi=\text{odd} \tag{6}$$

is called parity unfavored, where ΔL is the angular momentum transfer and $\Delta\Pi(=0$ or $1)$ is the change of parity. Fano showed [21] that the differential cross section for a parity unfavored state is zero at the scattering angles of 0° and 180°, and remains small for low scattering angles. This prediction is verified by the observation of the ''$2p^2$'' ${}^3P^e$ state, which does disappear when θ is 0° or 180° and is negligible at small scattering angles [10,22].

B. Overlapping resonances and state-state interference

A possible consequence of the overlapping of the resonances is the existence of state-state interference [2], which, although it potentially leads to considerable complications when analyzing the spectra, is expected to be negligible for the present data. The reason for this can be understood using the quantum-mechanical law that two processes will not interfere if we can, in principle, distinguish between their final states, even though we might not actually do so. Therefore, doubly excited states with different quantum numbers ${}^{2S+1}L^{\Pi}$ will not interfere, since these decay to distinguishable ionization states. In Sec. IV, it will be shown that the ${}^{2S+1}L^{\Pi}$ are different for all the states that are expected to have significant effects on the spectra and that are spaced closely in energy relative to their widths. Consequently, we have assumed that state-state interference has a negligible effect on the shapes of the resonance profiles, and so it is not included in the following data analysis. It is fortunate that state-state interference can be neglected, for otherwise the analysis of the spectra would be excessively complicated (see Sec. IV). The prediction is verified experimentally, since the spectra are well fitted using noninterfering resonance profiles of the Shore form.

C. Postcollision interactions

The interaction between the scattered and ejected electrons, which is known as postcollision interaction (PCI), can affect the position and shape of a resonance profile [23]. Since one of the aims of the experiment is to measure the energies and widths of the $N=3$ states, we need to estimate the magnitude of the PCI effects and determine whether these should be taken into account.

Using a classical model in which the approximation is made that the scattered and ejected electrons are thin spherical shells, it has been shown [24] that the PCI energy shift is given approximately by

$$\Delta E_{\mathrm{PCI}}(E_s,E_e)\approx\left[\frac{e^2m_e^{1/2}}{2^{5/2}\pi\varepsilon_o\hbar}\right]\left\{\frac{\Gamma(\sqrt{E_e}-\sqrt{E_s})}{\sqrt{E_e}\ \sqrt{E_s}}\right\},\quad E_e>E_s \tag{7}$$

where e is the electron charge, m_e is the electron mass, ε_o is the permittivity of free space, $\hbar$ is the Planck constant, and E_s and E_e are the energies of the scattered and ejected electrons, respectively. The energy shift is zero in this model when $E_e<E_s$.

The $N=3$ states can decay to the $\mathrm{He}^+(N=1)$ and $\mathrm{He}^+(N=2)$ channels by ejecting electrons with the energies of approximately 45 eV and 4 eV, respectively. In the experiments to be discussed the residual energies are 20 eV and 40 eV, and so only the 45 eV ejected electrons overtake the scattered electrons and hence cause a significant PCI effect. If Γ is given the typical value of 100 meV for the observed $N=3$ states, then Eq. (7) with E_e equal to 45 eV gives 27 meV and 3.3 meV for ΔE_{PCI} at the residual energies of 20 eV and 40 eV, respectively. To obtain the estimated PCI energy shifts, it is necessary to multiply these values for ΔE_{PCI} by the fraction for the $N=3$ states decaying to the $\mathrm{He}^+(N=1)$ channel. According to the measurements of Lindle *et al.* [25], the fraction for the ${}_3(1,1)_3^+\ {}^1P^o$ state is 0.021. Using the propensity rules for autoionization discussed in [17], in particular the result that $\Delta N=-1$ is strongly favored, suggests that approximately equal fractions would be obtained for the other $N=3$ states. The estimated PCI energy shifts at the residual energies of 20 eV and 40 eV are therefore 0.58 meV and 0.07 meV, respectively. Thus, according to our simplified model, the PCI energy shifts and the distortion of the shapes of the resonance profiles are neg-

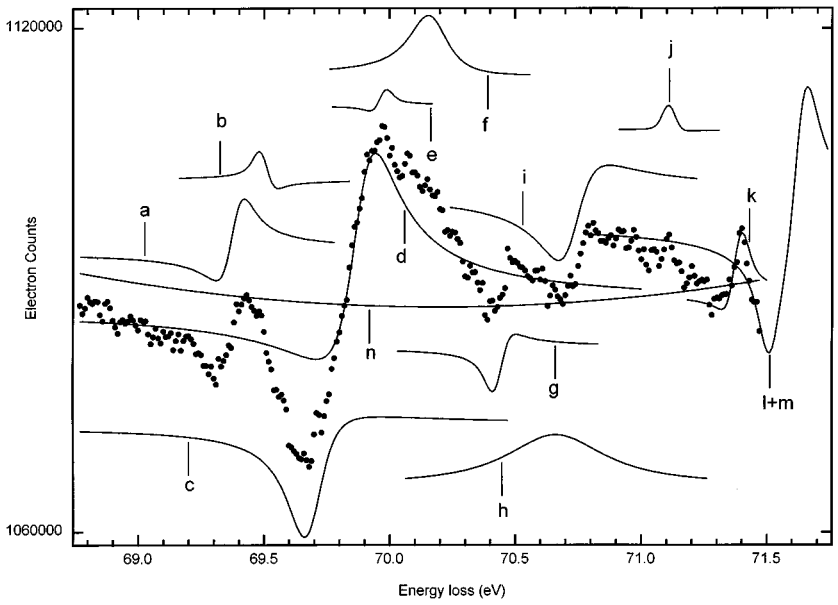

FIG. 3. The higher resolution $N=3$ data and the individual fits to the states at the residual energy of 40 eV and the scattering angle of 20°. The letters (a), (b), (c), (d), (e), (f), (g), (h), (i), (j), (k), (l), and (m) represent the states ${}_3(2,0)_3^+\ {}^1S^e$, ${}_3(2,0)_3^+\ {}^3P^o$, ${}_3(2,0)_3^+\ {}^1D^e$, ${}_3(1,1)_3^+\ {}^1P^o$, ${}_3(2,0)_3^+\ {}^3F^o$, ${}_3(1,1)_3^+\ {}^3D^e$, ${}_3(0,2)_3^+\ {}^1D^e$, ${}_3(2,0)_3^+\ {}^1G^e$, ${}_3(1,1)_3^+\ {}^1F^o$, ${}_3(0,0)_3^+\ {}^1D^e$, ${}_4(2,0)_3^+\ {}^1S^e$, ${}_4(2,0)_3^+\ {}^1D^e$, and ${}_4(1,1)_3^+\ {}^1P^o$, respectively, and (n) is the direct-ionization continuum. A linear slope has been removed for the purpose of illustration.

ligible. We therefore feel justified in omitting the effects of PCI from the following analysis.

IV. ANALYSIS OF THE SPECTRA

We interpret in detail the two spectra collected at the optimum conditions determined as described in Sec. II B. According to the calculations of Ho and co-workers [14], there are 37 and 26 states in the energy range of the spectra collected at the residual energies of 20 eV and 40 eV, respectively. Consequently, if all the states were to be included in the fitting procedure, then up to 151 parameters would need to be optimized. Therefore, considering the large overlap between the states, it would appear that the interpretation of the spectra is all but impossible. However, the number of states included in the fit can be reduced greatly using the arguments discussed in Sec. III A. The steps in the procedure are the following:

(1) The stages given in (i), (ii), and (iii) are expected to have negligible cross sections and so are excluded from the data analysis.

(i) States for which $\Delta A \neq 0$ when excited from the ground state (propensity rule 1).

(ii) The parity unfavored states.

(iii) For a given T, A, and ${}^{2S+1}L^{\Pi}$, the cross section reduces greatly with each decrease in K (propensity rule 2). Therefore if the state ${}_n(N-1-T,T)_3^+\ {}^{2S+1}L^{\Pi}$ with K equal to its maximum value [see Eq. (5)] does not have a large cross section, then all the states with smaller values of K, ${}_n(K_v,T)_3^+\ {}^{2S+1}L^{\Pi}$, will have negligible cross sections, where $K_v=N-3-T, \ldots, -(N-1-T)$.

(2) As a guide for the dependence on ${}^{2S+1}L^{\Pi}$, use the experimental spectra for the doubly excited states of helium below the $N=2$ threshold collected at the same conditions.

(3) Divide the remaining states into those expected to have a major or minor effect on the spectra. We use the fact that for a Rydberg series the amplitudes and shapes of the resonance profiles are approximately constant, but the width varies as n^{*-3}, where n^* is the effective principle quantum number [26].

(i) The major states are given in (a), (b), and (c). (a) The lowest member of a Rydberg series ($n=3$) with the maximum allowed K, $K_{\max}$, for a given ${}^{2S+1}L^{\Pi}$ (propensity rule 2). (b) If the state ${}_n(K,T)_3^+\ {}^{2S+1}L^{\Pi}$ has a large cross section, then the next higher member of the Rydberg series ${}_{n+1}(K,T)_3^+\ {}^{2S+1}L^{\Pi}$ is also a major state. (c) States with the maximum possible value of $T=N-1=2$ [see Eq. (5)] and the highest allowed value of $K=K_{\max}-2$ for this T (propensity rule 3).

(ii) The minor states are given in (a) and (b). (a) If the state ${}_n(K,T)_3^+\ {}^{2S+1}L^{\Pi}$ has a small cross section, then the next higher member of the Rydberg series ${}_{n+1}(K,T)_3^+\ {}^{2S+1}L^{\Pi}$ is a minor state. (b) If the state ${}_n(N-1-T,T)_3^+\ {}^{2S+1}L^{\Pi}$ with the maximum value of K has a very large cross section, then the state with the next lowest value of K, ${}_n(N-3-T,T)_3^+\ {}^{2S+1}L^{\Pi}$, may have a minor effect.

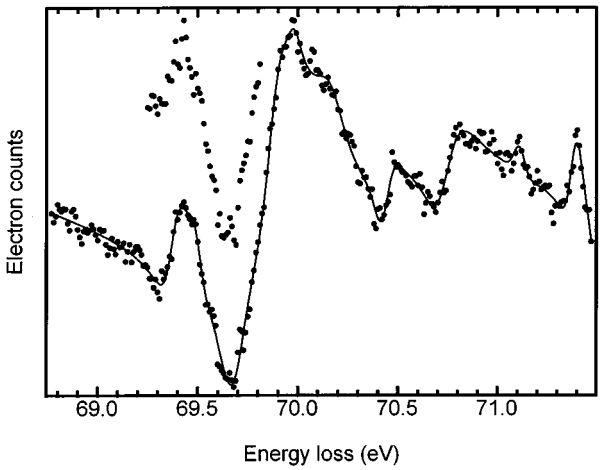

FIG. 4. The total fit to the $N=3$ data at the residual energy of 40 eV and the scattering angle of 20°. The inset is an independent spectrum collected over a reduced energy interval to confirm the separation of the ${}^1S^e$ and ${}^3P^o$ states.

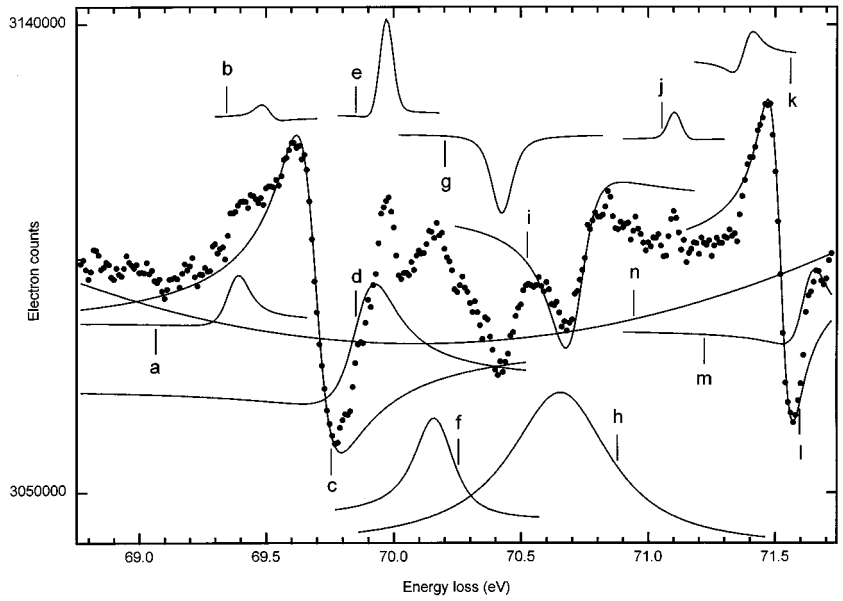

FIG. 5. The higher resolution $N=3$ data and the individual fits to the states at the residual energy of 20 eV and the scattering angle of 20°, where the same notation is used as in Fig. 3. A linear slope has been removed for the purpose of illustration.

The major states in the energy range of the 40 eV spectrum are therefore ${}_3(2,0)_3^+\ {}^1S^e$, ${}_3(2,0)_3^+\ {}^3P^o$, ${}_3(2,0)_3^+\ {}^1D^e$ ${}_3(1,1)_3^+\ {}^1P^o$, ${}_3(2,0)_3^+\ {}^3F^o$, ${}_3(1,1)_3^+\ {}^3D^e$, ${}_3(0,2)_3^+\ {}^1D^e$, ${}_3(2,0)_3^+\ {}^1G^e$, and ${}_3(1,1)_3^+\ {}^1F^o$. For the 20 eV spectrum, the ${}_4(2,0)_3^+\ {}^1D^e$ and ${}_4(1,1)_3^+\ {}^1P^o$ states should also be included. The minor states in the energy range of the 40 eV spectrum are ${}_3(0,0)_3^+\ {}^1D^e$, ${}_3(-1,1)_3^+\ {}^1P^o$, ${}_4(2,0)_3^+\ {}^1S^e$, and ${}_4(2,0)_3^+\ {}^3P^o$, whereas for the 20 eV spectrum we must also include the ${}_4(2,0)_3^+\ {}^3F^o$ state. A more detailed discussion of steps (1)–(3) is given in [27]. The elimination procedure is supported by the goodness of the fits obtained below.

We start by interpreting the spectrum collected at the residual energy of 40 eV and the scattering angle of 20° with the improved resolution of 58 ± 3 meV. The data and the individual fits to the states are shown in Fig. 3. The total fit to the spectrum is displayed in Fig. 4. The minor states ${}_3(-1,1)_3^+\ {}^1P^o$ and ${}_4(2,0)_3^+\ {}^3P^o$ and the ''anomalous'' ${}_3(0,0)_3^+\ {}^1S^e$ state are not clearly required, and so are excluded from the data analysis. To fit to the change in slope that begins at about 71.1 eV, it is necessary to include the ${}_4(2,0)_3^+\ {}^1D^e$ and ${}_4(1,1)_3^+\ {}^1P^o$ states outside the observed energy range, which are shown added together in Fig. 3. The fitting of 13 states to the spectrum requires the optimization of 55 parameters, which makes it difficult to find the unique solution. Therefore, although very much simplified by the elimination procedure, the data analysis is still a formidable task. It has, nevertheless, been possible to obtain fits in which the parameters always converge to the same values to within the quoted uncertainties, implying that the fit shown in Fig. 3 and that to be displayed in Fig. 5 are almost certainly the unique solutions. The number of degrees of freedom for the present analysis is 215, and so for a good fit χ^2 is approximately normally distributed with a mean value of 215 and a standard deviation of 21 [13]. The value of χ^2 obtained here is 239, and therefore the model adequately reproduces the data.

The energies and widths of the ${}_3(2,0)_3^+\ {}^1D^e$, ${}_3(2,0)_3^+\ {}^3F^o$, ${}_3(1,1)_3^+\ {}^3D^e$, ${}_3(2,0)_3^+\ {}^1G^e$, and ${}_4(2,0)_3^+\ {}^1D^e$ states can be measured more accurately at the residual energy of 20 eV than 40 eV, and so the values obtained at 20 eV were fixed in the fit to the 40 eV spectrum. Similarly, the energies and widths of the ${}^1P^o$ states are more easily determined for $N=3$ by photoionization experiments than by electron impact [4, 5, 28, 29]. Therefore, we used the data of [29] to deduce that $E_m[{}_3(1,1)_3^+\ {}^1P^o]=69.880$ eV, $\Gamma_m[{}_3(1,1)_3^+\ {}^1P^o]=191$ meV, $E_m[{}_4(1,1)_3^+\ {}^1P^o]=71.725$ eV and $\Gamma_m[{}_4(1,1)_3^+\ {}^1P^o]=75$ meV, and fixed the energies and widths equal to these values. Since there are few data points to optimize the parameters of the ${}_4(2,0)_3^+\ {}^1D^e$ and ${}_4(1,1)_3^+\ {}^1P^o$ states, it is necessary to fix the Shore A and B parameters for each of these states. The A and B parameters were chosen so that each resonance profile has an amplitude and shape equal to that of the corresponding lower member of the Rydberg series.

As a result of improving the resolution, the structure that appears as a single broad peak in Figs. 1 and 2 at about 69.4 eV is resolved into the ${}_3(2,0)_3^+\ {}^1S^e$ and ${}_3(2,0)_3^+\ {}^3P^o$ states.

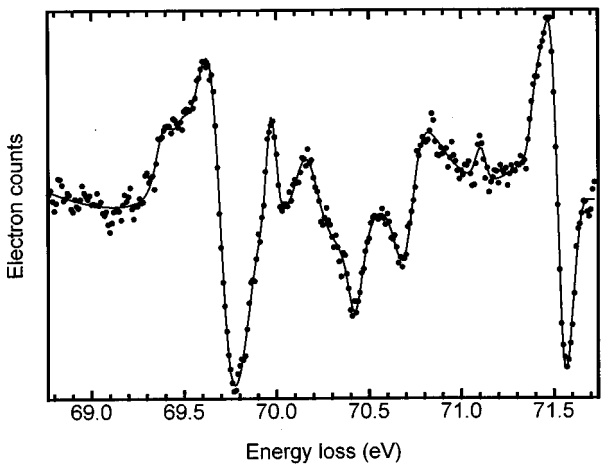

FIG. 6. The total fit to the $N=3$ data at the residual energy of 20 eV and the scattering angle of 20°.

To confirm the separation of the $^1S^e$ and $^3P^o$ states, an independent spectrum was collected in the reduced energy interval of 69.25–69.81 eV with a slightly improved resolution of 55 meV, and is displayed inset in Fig. 4.

We now interpret the spectrum collected at the residual energy of 20 eV and the scattering angle of 20° with the improved resolution of 60 ± 2 meV. The data and the individual fits to the states are shown in Fig. 5. The total fit to the spectrum is displayed in Fig. 6. The minor states $_3(-1,1)_3^+\ ^1P^o$, $_4(2,0)_3^+\ ^3P^o$, $_4(2,0)_3^+\ ^3F^o$, and the $_3(0,0)_3^+\ ^1S^e$ state are not clearly required, and so are excluded from the data analysis. The number of degrees of freedom is 242, and therefore the value obtained for χ^2 at 200, although slightly on the low side, implies that the fit is again acceptable. The energies and widths of the $_3(2,0)_3^+\ ^1S^e$, $_3(2,0)_3^+\ ^3P^o$, and $_4(2,0)_3^+\ ^1S^e$ states are fixed at the values obtained from the 40 eV spectrum. Also, E_m and Γ_m for the $^1P^o$ states are set equal to the same values as before.

The hardest aspect of the data analysis is the need to include ''hidden states,'' which are states that are not obviously present but nevertheless have an important underlying effect. The most surprising of the hidden states is the relatively large and very broad $_3(2,0)_3^+\ ^1G^e$ state, which is necessary in order to fit to the middle region of the spectrum. The first two members of the hidden $_n(1,1)_3^+\ ^1P^o$ Rydberg series are also revealed.

The spectra confirm the predictions of the propensity rules for K, T, and A. Comparing the relative cross sections of the $_3(2,0)_3^+\ ^1D^e$ and $_3(0,0)_3^+\ ^1D^e$ states shows that when K decreases from 2 to 0 the cross section reduces from the largest in the spectrum to a small and narrow feature, which is as expected according to the K propensity rule. Also, the cross section of the $_3(0,2)_3^+\ ^1D^e$ state is larger than that of the $_3(0,0)_3^+\ ^1D^e$ state, which verifies the T propensity rule. Further, the states $_3(2,0)_3^+\ ^1D^e$ and $_3(0,2)_3^+\ ^1D^e$ show that the effect of K on the cross section is greater than that of T. Finally, no states with $A=-1$ or 0 are observed, and so the propensity rule $\Delta A=0$ applies strictly. The absence of a clear resonance profile due to the ''anomalous'' $_3(0,0)_3^+\ ^1S^e$ state indicates a possible difference between propensity rules for the present experiments and those for autoionization.

One of the most unexpected results in the $N=3$ data is the sudden increase in the relative cross section, and alteration in the shape, of the $_n(2,0)_3^+\ ^1D^e$ Rydberg series when the residual energy is reduced from 40 eV to 20 eV. It would be interesting to understand the cause of this large change in the relative cross sections of the $_n(2,0)_3^+\ ^1D^e$ states.

In Figs. 3 and 5, the positive quadratic variation in $C(E)$ [see Eq. (2)] as a function of the energy loss is not as would be expected due to changes in the focusing of the electron lenses, and is therefore probably a feature of the differential cross section of the direct-ionization continuum.

V. COMPARISON BETWEEN THE MEASURED AND THEORETICAL ENERGIES AND WIDTHS

Table I, the measured and theoretical energies and widths are compared, where (a) and (b) distinguish the parameters determined at the residual energies of 20 eV and 40 eV, respectively. To convert the theoretical energies into eV above the ground state, the reduced Rydberg energy of 13.6038 eV and the ground-state energy of $-2.903\,78$ a.u. are used. For the $^1P^o$ states in Table I, the measured values are deduced from [29], and the theoretical results are, for brevity, shown for only [14].

We will now comment on the parameters for which there is a significant disagreement between experiment and theory. There is a general tendency for the theoretical energies of the $_3(2,0)_3^+\ ^1D^e$, $_4(2,0)_3^+\ ^1S^e$, and $_4(2,0)_3^+\ ^1D^e$ states to be lower than the measured values. The values of $\Gamma_t[_3(1,1)_3^+\ ^3D^e]$, $\Gamma_t[_3(0,2)_3^+\ ^1D^e]$, and $\Gamma_t[_3(1,1)_3^+\ ^1F^o]$ are, respectively, smaller, larger, and smaller than the experimental results. The χ^2 is a minimum for $\Gamma_m[_3(0,0)_3^+\ ^1D^e]\approx0$ meV and increases by 1 when $\Gamma=6$ meV [see Eq. (3)], which suggests that $\Gamma_t[_3(0,0)_3^+\ ^1D^e]$ is much larger than the correct value. However, due to the low statistical accuracy of the $_3(0,0)_3^+\ ^1D^e$ resonance profile, χ^2 versus $(\Gamma-\Gamma_m)$ is approximately linear rather than the expected quadratic dependence, and so the estimated error might not be reliable. The $_3(2,0)_3^+\ ^3P^o$ resonance profile is small, apparently narrow and is located awkwardly between the relatively large profiles of the $_3(2,0)_3^+\ ^1S^e$ and $_3(2,0)_3^+\ ^1D^e$ states, which causes a large error in its width. Unfortunately, it was therefore impossible to obtain $\Gamma_m[_3(2,0)_3^+\ ^3P^o]$ with sufficient accuracy to allow for a precise test of the predicted widths. Thus, in general, the agreement between experiment and theory is quite good for the energies but poorer for the widths.

VI. THE n DEPENDENCE OF THE CROSS SECTION FOR THE $_n(n-1,0)_n^+\ ^1S^e$ STATES AND ELECTRON CORRELATIONS

Most of the authors who analyze the n dependence of the partial widths or cross sections for the Wannier ridge states ($\underline{r}_1\approx-\underline{r}_2$) only consider the states $_n(n-1,0)_n^+\ ^1S^e$, and so for comparison purposes only these states will be discussed here. For brevity, the $_n(n-1,0)_n^+\ ^1S^e$ states will, in this section, be referred to by the more familiar but less accurate notation ns^2. In the present experiments, only the $2s^2$ and $3s^2$ states are observed and therefore it is not the n dependence of the full ns^2 series that is determined, but the variation when n changes from 2 to 3.

A number of authors [44–48] have calculated the partial widths $\Gamma_n^{(g)}$ for the decay of the $He^-1s(ns^2)\ ^2S$ and $H^-(ns^2)\ ^1S$ series to the He $(1s^2)$ and H $(1s)$ channels, respectively. Writing

$$\Gamma_n^{(g)}\propto n^{-\alpha} \tag{8}$$

the following values of α have been obtained from classical and semiclassical treatments: 6 [44]; 5.254 [45]; 6.254 [46]; and 3.254 [47]. More recent, fully quantum-mechanical results by Chrysos *et al.* [48] for H^- and by Heim and Rau [49] for He (ns^2) have given $\alpha=6.8\pm0.4$ and $\alpha=6.5$, respectively.

We provide some insight into the relation between the value for α and electron-electron correlations. A similar ar-

TABLE I. The comparison between the measured (subscript m) and theoretical (subscript t) energies and widths. The labels (a) and (b) distinguish the parameters obtained at the residual energies of 20 eV and 40 eV, respectively. For the $^1P^o$ states, the values are deduced from the measurements of Zubek *et al.* [29].

State	E_m (eV)	E_t (eV)	Γ_m (meV)	Γ_t (meV)	Ref.
$_3(2,0)_3^+$ $^1S^e$	(b) 69.378±0.011	69.386	(b) 72±21	82	[14]
		69.386		88	[30]
		69.384		83	[31]
		69.386		82	[32]
		69.374			[34]
		69.380			[36]
		69.404			[37]
		69.404			[38]
		69.384		82	[39]
		69.377			[41]
		69.361			[42]
		69.392		83	[43]
$_3(2,0)_3^+$ $^3P^o$	(b) 69.498±0.020	69.472	(b) 0–130	81	[14]
		69.478		87	[30]
		69.471		85	[31]
		69.472		81	[32]
		69.475		77	[33]
		69.479		26	[35]
		69.479		82	[39]
		69.471			[40]
		69.451			[41]
		69.436			[42]
		69.479		116	[43]
$_3(2,0)_3^+$ $^1D^e$	(a) 69.686±0.005	69.668	(a) 145±11	140	[14]
		69.670		147	[30]
		69.679		147	[31]
		69.668		140	[32]
		69.615		136	[39]
		69.643			[41]
		69.624			[42]
		69.686		154	[43]
$_3(1,1)_3^+$ $^1P^o$	69.880±0.022	69.874	191±2	191	[14]
$_3(2,0)_3^+$ $^3F^o$	(a) 69.969±0.008	69.982	(a) $\leqslant$17	$<$0.014	[14]
		69.985		3	[30]
		69.982		0.85	[32]
		69.959			[41]
$_3(1,1)_3^+$ $^3D^e$	(a) 70.167±0.026	70.154	(a) 165±48	20	[14]
		70.162		21	[30]
		70.154		23	[31]
		70.154		20	[32]
		70.133			[41]
		70.119			[42]
$_3(0,2)_3^+$ $^1D^e$	(b) 70.433±0.010	70.420	(b) 38±18	117	[14]
		70.426		118	[30]
		70.420		117	[32]
		70.447			[41]
		70.433			[42]
$_3(2,0)_3^+$ $^1G^e$	(a) 70.66±0.12	70.651	(a) 470±280	182	[14]
		70.651		181	[30]
		70.649		180	[32]

TABLE I. (*Continued*).

State	E_m (eV)	E_t (eV)	Γ_m (meV)	Γ_t (meV)	Ref.
$_3(1,1)_3^+\ ^1F^o$	(b) 70.730±0.016	70.728	(b) 162±24	88	14
		70.733		89	30
		70.728		88	32
		70.738			41
$_3(0,0)_3^+\ ^1D^e$	(a) 71.105±0.015	71.112	(a) ⩽6	34	14
		71.127		35	30
		71.117		33	31
		71.113		34	32
		71.112			41
		71.099			42
$_4(2,0)_3^+\ ^1S^e$	(b) 71.382±0.007	71.358	(b) 22±11	41	14
		71.394		40	30
		71.356		37	31
		71.360			34
		71.420			38
		71.357		20	39
		71.362			41
		71.347			42
		71.384			43
$_4(2,0)_3^+\ ^1D^e$	(a) 71.519±0.004	71.502	(a) 56±7	65	14
		71.519		59	30
		71.494		62	31
		71.495			41
		71.480			42
$_4(1,1)_3^+\ ^1P^o$	71.625±0.022	71.627	75±2	79	14

gument is given in more detail in [49] and applies only to low values of n, such as the $n=2$ and $n=3$ measured in the present experiments, rather than to the (core) ns^2 series or threshold region. In the independent-particle model, the electrons are uncorrelated and the wave function is the product of two ns eigenfunctions, which would give a value of 6 for α. To represent an increase in the angular correlations, the proportion of the higher l components, $(nl^2)\ ^1S^e$, in the partial-wave expansion of $\psi(ns^2)$ rises [50], which causes the amplitude of the wave function in the center of the atom and, hence, the cross section to reduce. Therefore if angular correlations increase with n, then the cross section reduces more rapidly than according to the independent-particle model, which can be represented by writing

$$\sigma(ns^2) \propto n^{-[6+C(n)]}. \tag{9}$$

Thus, for low n, a value of $C(n)>0$ implies that electron correlations increase with n, and the larger is $C(n)$ the greater the rate of increase. We differ from [49] in that C is written as a function of n (see the discussion below).

To measure the total cross section $\sigma(3s^2)$ would require the collection of spectra at many different angles with the resolution of about 60 meV necessary to separate the $3s^2$ and $_3(2,0)_3^+\ ^3P^o$ states. This procedure would be excessively time consuming, and so the ratio of the cross sections was measured at only one scattering angle. The $2s^2$ and $3s^2$ states should be compared at the same scattering angle and energy above threshold, which are chosen as 20° and 40 eV since these are the conditions at which the $3s^2$ state appears most clearly in the present experiments. The $2s^2$ state was observed in a separate experiment, and a fit to its approximately Lorentzian peak gives $E_m=57.853\pm0.005$ eV and $\Gamma_m=115\pm2$ meV.

If the resonance profiles have a Lorentzian form when the broadening effects of the spectrometer are removed, then the cross section is proportional to the area under the Lorentzian curve, that is,

$$\frac{d\sigma^2(ns^2)}{dE\,d\Omega} \propto h(ns^2)\Gamma(ns^2), \tag{10}$$

where $h(ns^2)$ is the maximum height of the Lorentzian. To estimate the relative cross sections of the ns^2 states Eq. (10) is used, where for the slightly asymmetric profiles the vertical separation between the maximum and minimum of the resonance structure or amplitude is substituted for $h(ns^2)$. The mutual normalization of the $2s^2$ and $3s^2$ states is performed using the direct-ionization continuum. The amplitudes of the unbroadened resonance structures relative to the continuum cross section obtained from the fitting procedure are

$$h(2s^2)/\sigma_c(97.85) = 0.3640\pm0.0048, \tag{11}$$

$$h(3s^2)/\sigma_c(109.38) = 0.0109\pm0.0032, \tag{12}$$

where $\sigma_c(97.85)$ and $\sigma_c(109.38)$ are the double differential cross sections for the electron-impact ionization of helium, $d^2\sigma/dEd\Omega$, at incident energies of 97.85 eV and 109.38 eV, respectively, and at the same residual energy of 40 eV and scattering angle of 20°. If the approximation is made that σ_c varies linearly with impact energy for small extrapolations from the measured values of [51], then we obtain

$$\sigma_c(97.85)/\sigma_c(109.38)=1.11. \tag{13}$$

We have also calculated this ratio using the data of other authors [52–54] and have found the agreement to be within a few percent.

Combining Eqs. (10) to (13), and using the measured widths of the $2s^2$ and $3s^2$ states, yields

$$\frac{d^2\sigma(3s^2)}{dEd\Omega}\Bigg/\frac{d^2\sigma(2s^2)}{dEd\Omega}=0.017\pm0.005. \tag{14}$$

If the ratio of the differential cross sections (14) is representative of $\sigma(3s^2)/\sigma(2s^2)$, then this would imply a value of 10.1 ± 0.8 for α when n changes from 2 to 3. The theoretical values for α quoted above and that predicted by the independent-particle model are significantly smaller than 10.1. However, the above theories apply to the (core) ns^2 series and in some cases to the threshold region, rather than to the low values of $n=2$ and $n=3$ measured in the present experiments. A possible explanation for the discrepancy is therefore suggested by the measurements of Buckman and Newman [55] and the calculations of Chrysos *et al.* [48], which show that α reduces as n increases. Such a decrease in α is expected, since there is a large initial increase in electron-electron correlations as the effects of the nucleus rapidly lose their dominance, after which in the higher n region the correlation pattern becomes well established. The discrepancy cannot be due to the higher effective charge Z^* of the core for He(ns^2) than for the systems considered in [44–48], since α is expected to reduce as Z^* increases. Thus, the value for α obtained in the present experiments suggests that there is a large increase in electron correlations when n rises from 2 to 3.

VII. SUMMARY

Measurements of the doubly excited states of helium below the $He^+(N=3)$ threshold populated by electron impact have been presented for a range of scattering angles and residual energies. The agreement between the measured energies obtained and the theoretical values is generally good, although there are a few small discrepancies for most of the calculations. For the states ${}_3(1,1)_3^+\ {}^3D^e$, ${}_3(0,2)_3^+\ {}^1D^e$, and ${}_3(1,1)_3^+\ {}^1F^o$ the differences between the measured and theoretical widths are large and greater than the experimental errors, where the errors include statistical inaccuracy, nonuniqueness in the fitting procedure and the uncertainty in the energy resolution. There are two further possible sources of error, namely, the correct choice of states to include in the fitting procedure and state-state interference, but we expect on the basis of our arguments and the goodness of the fits obtained that these have negligible effect on the measured widths.

We have also investigated in two ways how the correlations between the two excited electrons affects the cross section of the doubly excited states of helium. First, the data verifies propensity rules in Lin's K,T,A classification scheme for the cross sections, and thus shows how the excitation probability depends on the radial and angular correlations. Second, by comparing the $2s^2\ {}^1S^e$ and $3s^2\ {}^1S^e$ states at the scattering angle of 20° and the residual energy of 40 eV, we obtained a dependence of $n^{-10.1\pm0.8}$ for the differential cross section at these conditions. If these differential cross sections are representative of the total cross sections σ, then σ reduces more rapidly when n changes from 2 to 3 than according to theoretical predictions. We suggest that the discrepancy is due to an atypically large increase in electron-electron correlations when n rises from 2 to 3, which causes the cross section to reduce more rapidly than according to the theoretical calculations that apply to the (core) ns^2 series or threshold region.

[1] U. Fano and A. R. P. Rau, *Atomic Collisions and Spectra* (Academic, Orlando, 1986), Chap. 10.

[2] U. Fano, Phys. Rev. **124**, 1866 (1961).

[3] R. P. Madden and K. Codling, Phys. Rev. Lett. **10**, 516 (1963); Astrophys. J. **141**, 364 (1965).

[4] P. R. Woodruff and J. A. R. Samson, Phys. Rev. A **25**, 848 (1982).

[5] M. Domke, K. Schulz, G. Remmers, G. Kaindl, and D. Wintgen, Phys. Rev. A **53**, 1424 (1996).

[6] P. J. Hicks and J. Comer, J. Phys. B **8**, 1866 (1975); J. P. van den Brink, G. Nienhuis, J. van Eck, and H. G. M. Heideman, J. Phys. B **22**, 3501 (1989).

[7] P. Hammond, G. C. King, J. Jureta, and F. H. Read, J. Phys. B **18**, 2057 (1985); A. D. Bass, Ph.D thesis, University of Manchester, 1988.

[8] E. Harting and F. H. Read, *Electrostatic Lenses* (Elsevier, Amsterdam, 1976).

[9] J. V. Hatfield, S. A. Burke, J. Comer, F. Currell, J. Goldfinch, T. A. York, and P. J. Hicks, Rev. Sci. Instrum. **63**, 235 (1992).

[10] V. Srigengan, Ph.D. thesis, University of Manchester, 1992.

[11] B. W. Shore, Phys. Rev. **171**, 43 (1968).

[12] D. W. Marquardt, J. Soc. Ind. Appl. Math. **11**, 431 (1963).

[13] P. R. Bevington, *Data Reduction and Error Analysis for the Physical Sciences* (McGraw-Hill, New York, 1969).

[14] Y. K. Ho and J. Callaway, J. Phys. B **18**, 3481 (1985); Y. K. Ho, *ibid.* **34**, 4402 (1986); Y. K. Ho and A. K Bhatia, *ibid.* **44**, 2895 (1991); Y. K. Ho, *ibid.* **44**, 4154 (1991); Y. K. Ho and A. K. Bhatia, *ibid.* **47**, 2628 (1993); Y. K. Ho, *ibid.* **48**, 3598 (1993).

[15] J. M. Rost and J. S. Briggs, J. Phys. B **23**, L339 (1990); **24**, 4293 (1991).
[16] A. Vollweiter, J. M. Rost, and J. S. Briggs, J. Phys. B **24**, L155 (1991).
[17] S. Watanabe and C. D. Lin, Phys. Rev. A **34**, 823 (1986).
[18] H. R. Sadeghpour and C. H. Greene, Phys. Rev. Lett. **65**, 313 (1990).
[19] C. D. Lin, Adv. At. Mol. Phys. **22**, 77 (1986).
[20] D. R. Herrick and O. Sinanoglu, Phys. Rev. A **11**, 97 (1975).
[21] U. Fano, Phys. Rev. **135**, B863 (1964).
[22] H. B. van Linden van den Heuvell, W. van de Water, H. G. M. Heideman, J. van Eck, and L. Moorman, J. Phys. B **13**, 2475 (1980).
[23] M. Yu. Kuchiev and S. A. Sheinerman, Usp. Fiz. Nauk. **158**, 353(1989) [Sov. Phys. Usp. **32**, 569 (1989)].
[24] G. N. Ogurtsov, J. Phys. B **16**, L745 (1983).
[25] D. W. Lindle, T. A. Ferrett, P. A. Heimann, and D. A. Shirley, Phys. Rev. A **36**, 2112 (1987).
[26] U. Fano and J. W. Cooper, Phys. Rev. A **137**, 1364 (1965).
[27] S. J. Brotton, Ph.D. thesis, University of Manchester, 1994.
[28] H. Kossmann, B. Krassig, and V. Schmidt, J. Phys. B **21**, 1489 (1988).
[29] M. Zubek, G. C. King, P. M. Rutter, and F. H. Read, J. Phys. B **22**, 3411 (1989); M. Zubek, G. Dawber, R. I. Hall, L. Avaldi, K. Ellis, and G. C. King, J. Phys. B **24**, L337 (1991).
[30] L. Quigley and K. Berrington, J. Phys. B (to be published).
[31] W. C. Fon, K. Ratnavelu, K. M. Aggarwal, and K. A. Berrington, J. Phys. B **27**, L803 (1994).
[32] E. Lindroth, Phys. Rev. A **49**, 4473 (1994).
[33] I. Sanchez and F. Martin, Phys. Rev. A **47**, 1878 (1993).
[34] G. S. Ezra, K. Richter, G. Tanner, and D. Wintgen, J. Phys. B **24**, L413 (1991).
[35] L. Wu and J. Xi, J. Phys. B **23**, 727 (1990).
[36] J. M. Rost and J. S. Briggs, J. Phys. B **22**, 3587 (1989).
[37] J. M. Rost and J. S. Briggs, J. Phys. B **21**, L233 (1988).
[38] N. Koyama, H. Fukuda, T. Motoyama, and M. Matsuzawa, J. Phys. B **19**, L331 (1986).
[39] S. Wakid and J. Callaway, Phys. Lett. **78A**, 137 (1980).
[40] K. T. Chung and B. F. Davis, Phys. Rev. A **22**, 835 (1980).
[41] L. Lipsky, R. Anania, and M. J. Conneely, At. Data. Nucl. Data. Table **20**, 127 (1977).
[42] R. S. Oberoi, J. Phys. B **5**, 1120 (1972).
[43] P. G. Burke and A. J. Taylor, J. Phys. B **2**, 44 (1969).
[44] A. R. P. Rau, J. Phys. B **16**, L699 (1983).
[45] J. M. Feagin and J. Macek, J. Phys. B **17**, L245 (1984); J. Macek and J. M. Feagin, J. Phys. B **18**, 2161 (1985).
[46] A. R. P. Rau, in *Atomic Physics 9*, edited by R. S. Van Dyck, Jr. and E. N. Fortson (World Scientific, Singapore, 1989), p. 491.
[47] S. Cvejanovic, Z. Dohcevic, and P. Grujic, J. Phys. B **23**, L167 (1990).
[48] M. Chrysos, Y. Komninos, Th. Mercouris, and C. A. Nicolaides, Phys. Rev. A **42**, 2634 (1990).
[49] T. A. Heim and A. R. P. Rau, J. Phys. B **28**, 5309 (1995).
[50] A. R. P. Rau, J. Phys. B **17**, L75 (1984); A. R. P. Rau and Q. Molina, J. Phys. B **22**, 189 (1989).
[51] R. Müller-Fiedler, K. Jung, and H. Ehrhardt, J. Phys. B **19**, 1211 (1986).
[52] T. W. Shyn and W. E. Sharp, Phys. Rev. A **19**, 557 (1979).
[53] M. E. Rudd and R. D. Dubois, Phys. Rev. A **16**, 26 (1977).
[54] Y. K. Kim, Phys. Rev. A **28**, 656 (1983).
[55] S. J. Buckman and D. S. Newman, J. Phys. B **20**, L711 (1987).